

# Theoretical study of the absorption spectra of the lithium dimer

H.-K. Chung, K. Kirby, and J. F. Babb

*Institute for Theoretical Atomic and Molecular Physics,*

*Harvard-Smithsonian Center for Astrophysics,*

*60 Garden Street, Cambridge, MA 02138*

## Abstract

For the lithium dimer we calculate cross sections for absorption of radiation from the vibrational-rotational levels of the ground  $X^1\Sigma_g^+$  electronic state to the vibrational levels and continua of the excited  $A^1\Sigma_u^+$  and  $B^1\Pi_u$  electronic states. Theoretical and experimental data are used to characterize the molecular properties taking advantage of knowledge recently obtained from photoassociation spectroscopy and ultra-cold atom collision studies. The quantum-mechanical calculations are carried out for temperatures in the range from 1000 to 2000 K and are compared with previous calculations and measurements.

PACS numbers: 33.20.-t, 34.20.Mq, 52.25.Rv

## I. INTRODUCTION

The absorption spectra of pure alkali-metal vapors at temperatures of the order 1000 K can be a rich source of information on molecular potentials and properties. Achieving a high vapor pressure of lithium in experiments requires higher temperatures than the other alkali-metal atoms, but there are some data from heat pipe ovens [1–3] and from a specialized apparatus [4]. In addition to the atomic lines the spectra exhibit gross molecular features attributable to transitions between bound levels of the ground electronic state and levels of the excited singlet states and weaker features arising from analogous triplet transitions.

Theoretically, the envelope of the alkali-metal molecular absorption spectra can be quantitatively reproduced using semi-classical models [5–9] and ro-vibrational structure [7] and continua [10] can be reproduced from quantum-mechanical models. In this paper we calculate quantum-mechanically absorption spectra for the  $X^1\Sigma_g^+ - A^1\Sigma_u^+$  and  $X^1\Sigma_g^+ - B^1\Pi_u$  transitions in  $\text{Li}_2$ . Although both semi-classical [7] and quantum-mechanical [7,11] calculations have been performed and compared [7] previously for these transitions of  $\text{Li}_2$ , recent improvements in the molecular data prompt the present comprehensive study.

From photoassociation spectroscopy and cold collision studies performed in the last few years as well as recent theoretical work there have been significant critical tests of and improvements to the molecular potentials [12–14], particularly at long-range [15–17], and transition dipole moment data [15] available for  $\text{Li}_2$ , as well as to the value of the lifetime of the  $\text{Li } 2p$  state [18,19]. This paper presents calculations of the spectra over the full range of wavelengths where absorption in the  $X^1\Sigma_g^+ - A^1\Sigma_u^+$  and  $X^1\Sigma_g^+ - B^1\Pi_u$  bands is possible. We calculate the satellite feature profiles at various temperatures, identify and explore the influence of quasibound states and the contributions of bound–bound versus bound–free transitions, calculate partition functions, and calculate lifetimes for the  $A^1\Sigma_u^+$  and  $B^1\Pi_u$  ro-vibrational levels.

## II. QUANTUM THEORY OF ABSORPTION CROSS SECTION

In the quantum-mechanical formulation an absorption cross section from a vibration-rotation state of the lower electronic state ( $v'', J'', \Lambda''$ ) to the vibration-rotation state of the upper electronic state ( $v', J', \Lambda'$ ) is

$$\sigma_{v''J''\Lambda''}^{v'J'\Lambda'}(\nu) = \frac{8\pi^3\nu}{3hc} |\langle \phi_{v''J''\Lambda''} | D(R) | \phi_{v'J'\Lambda'} \rangle|^2 g(\nu - \nu_{ij}) \frac{S_{J''\Lambda''}^{J'\Lambda'}}{2J'' + 1} \quad (1)$$

where  $g(\nu - \nu_{ij})$  is a line-shape function of dimension  $\nu^{-1}$ ,  $S_{J''\Lambda''}^{J'\Lambda'}$  is the Hönl-London factor and  $\nu_{ij} \equiv |E_{v'J'\Lambda'} - E_{v''J''\Lambda''}|$  is the transition frequency [20,21]. In this study,  $g(\nu - \nu_{ij})$  is approximated by  $1/\Delta\nu$ , with  $\Delta\nu$  the bin size. For a bound-free transition, the absorption cross section from a bound level of the lower electronic state ( $v''J''\Lambda''$ ) to a continuum level of the upper electronic state ( $\epsilon'J'\Lambda'$ ) can be written as

$$\sigma_{v''J''\Lambda''}^{\epsilon'J'\Lambda'}(\nu) = \frac{8\pi^3\nu}{3hc} |\langle \phi_{v''J''\Lambda''} | D(R) | \phi_{\epsilon'J'\Lambda'} \rangle|^2 \frac{S_{J''\Lambda''}^{J'\Lambda'}}{2J'' + 1} \quad (2)$$

where the continuum wave function  $\phi_{\epsilon'J'\Lambda'}$  is energy normalized. Free-bound or free-free transitions are not considered since the temperatures studied here are not high enough for these types of transitions to be important within the singlet manifold.

The radial wave function can be obtained from the Schrödinger equation for the relative motion of the nuclei

$$\frac{d^2\phi(R)}{dR^2} + \left( \frac{2\mu}{\hbar^2}E - \frac{2\mu}{\hbar^2}V(R) - \frac{J(J+1) - \Lambda^2}{R^2} \right) \phi(R) = 0, \quad (3)$$

where  $V(R)$  is the rotationless potential energy for the electronic state,  $\mu = 6394.7$  is the reduced mass of the  ${}^7\text{Li}$  atoms, and  $E$  is for bound states the eigenvalue  $E_{vJ\Lambda}$  measured with respect to the dissociation limit associated with the wave function  $\phi(R) = \phi_{vJ\Lambda}(R)$ . Similarly, for continuum states  $E$  is the relative kinetic energy of the colliding atoms  $E_{\epsilon J\Lambda}$  associated with the energy-normalized wave function  $\phi(R) = \phi_{\epsilon J\Lambda}(R)$ .

The total absorption cross section at frequency  $\nu$  can be obtained by averaging over initial vibration-rotation levels ( $v''$ ,  $J''$ ,  $\Lambda''$ ) with a relevant weighting factor and summing over all possible bound-bound and bound-free transitions with frequencies between  $\nu$  and  $\nu + \Delta\nu$  [7] yielding

$$\sigma(\nu) = Z_l^{-1} \left[ \sum_{J'', \Lambda'', v''} \sigma_{v''J''\Lambda''}^{v'J'\Lambda'} \omega_{J''} (2J'' + 1) \exp[-(D_e + E_{v''J''\Lambda''})/kT] + \sum_{J'', \Lambda'', v''} \int d\epsilon' \sigma_{v''J''\Lambda''}^{\epsilon'J'\Lambda'} \omega_{J''} (2J'' + 1) \exp[-(D_e + E_{v''J''\Lambda''})/kT] \right], \quad (4)$$

where  $\omega_{J''}$  is a statistical factor due to nuclear spin with the values  $[I/(2I+1)] = \frac{3}{8}$  for even  $J$  and  $[(I+1)/(2I+1)] = \frac{5}{8}$  for odd  $J$ , for  ${}^7\text{Li}_2$  with  $I = \frac{3}{2}$ . With the zero of energy taken to be the potential minimum, the partition function  $Z_l$  of the lower state with dissociation energy  $D_e$  is

$$Z_l = \sum_{J'', \Lambda'', v''} \omega_{J''} (2J'' + 1) \exp[-(D_e + E_{v''J''\Lambda''})/kT], \quad (5)$$

assuming thermodynamic equilibrium. The resulting cross sections can be used to model the dimer absorption spectra in the quasistatic limit.

### III. MOLECULAR DATA

The adopted molecular potentials of the  $X^1\Sigma_g^+$ ,  $A^1\Sigma_u^+$  and  $B^1\Pi_u$  states are shown in Fig. 1. The ground  $X^1\Sigma_g^+$  state potential was constructed using the approach of Ref. [22]. We adopted the recommended [23] potential obtained by Barakat *et al.* [24], who applied the Rydberg-Klein-Rees (RKR) method to measured energies. The data were connected smoothly to the long-range form

$$V(R) = -\frac{C_6}{R^6} - \frac{C_8}{R^8} - \frac{C_{10}}{R^{10}} + V_{\text{exc}}(R), \quad (6)$$

where  $V_{\text{exc}}(R)$  is the exchange energy [22] and the coefficients  $C_6$ ,  $C_8$ , and  $C_{10}$  have been calculated in Refs. [15,25–27] and we use atomic units in this section. We adopted the coefficients  $C_6 = 1\,393.39$ ,  $C_8 = 83\,425.8$  and  $C_{10} = 7.372 \times 10^6$  from Ref. [26]. The two regions were connected at  $R = 23.885 a_0$  yielding a value of  $8516.95 \text{ cm}^{-1}$  for the dissociation energy of the  $X^1\Sigma_g^+$  state of  ${}^7\text{Li}_2$ , in satisfactory agreement with the accepted value of  $8516.61 \text{ cm}^{-1}$  [23]. The form  $a \exp(-bR)$  was used to extrapolate the potential at short-range where the constants were determined to smoothly connect to the innermost RKR points. The resulting  $X^1\Sigma_g^+$  potential yields an  $s$ -wave scattering length of  $33.6 a_0$ , in excellent agreement with the accepted [28] value of  $33 \pm 2$  and a sensitive test of the assembled data.

For the excited  $A^1\Sigma_u^+$  state the RKR potential of Ref. [17] was adopted and smoothly connected at about  $R = 140 a_0$  to the long-range form

$$V(R) = \frac{C_3}{R^3} - \frac{C_6}{R^6} - \frac{C_8}{R^8}, \quad (7)$$

with coefficients  $C_3 = -11.000\,226$  and  $C_6 = 2\,075.05$  from Ref. [26] and  $C_8 = 2.705 \times 10^5$  from Ref. [15]. For  $R < 3.78 a_0$  the data were connected to the short range form  $a \exp(-bR)$ . The dissociation energy for the  $A^1\Sigma_u^+$  state is determined to be  $9\,352.194 \text{ cm}^{-1}$  in our calculation, in good agreement with the experimental value [29] of  $9\,352.5(6) \text{ cm}^{-1}$  given in Ref. [30].

The potential for the  $B^1\Pi_u$  state has a hump with maximum at  $R \approx 11 a_0$  and various determinations of the hump location and height have been summarized in Refs. [31] and [30]. We adopted the IPA (Inverted Perturbation Approach) potentials from Hessel and Vidal [32] for  $R < 9.35 a_0$  and the *ab initio* potential of Schmidt-Mink *et al.* [30] for  $10.5 < R < 30 a_0$  with one additional point at  $R = 11.2 a_0$  fixing the barrier maximum energy at  $512 \text{ cm}^{-1}$  above dissociation. At  $R = 30 a_0$  the data were connected to the long-range form of Eq. (7) by shifting down the data by  $0.3 \text{ cm}^{-1}$  from  $10.5 < R < 30$ . The values of the coefficients

used in Eq. (7) were  $C_3 = 5.500\,113$  and  $C_6 = 1406.08$  from Ref. [26] and  $C_8 = 4.756 \times 10^4$  from Ref. [15]. The potential energy data for  $R < 9.35 a_0$  were fixed using the  $B^1\Pi_u$  state dissociation energy of  $2\,984.8 \text{ cm}^{-1}$ , which we determined using the experimental value for  $T_e$  of  $20\,436.32 \text{ cm}^{-1}$  [32], the atomic asymptotic energy of  $14\,904.0 \text{ cm}^{-1}$ , and the  $X^1\Sigma_g^+$  dissociation energy of  $8\,516.61 \text{ cm}^{-1}$  [23]. Finally, the data in the range  $9.35 < R < 10.5$  were smoothly connected using cubic splines. For  $R < 4.254\,61 a_0$  the data were extrapolated using the short range form  $a \exp(-bR)$ .

Transition dipole moments for the  $X^1\Sigma_g^+ - A^1\Sigma_u^+$  and  $X^1\Sigma_g^+ - B^1\Pi_u$  transitions are available from *ab initio* calculations [33,34,30] and for X–A transitions from measured lifetimes of A state levels [35]. For the electronic transition dipole moments  $D(R)$ , we adopted *ab initio* calculations of Ratcliff, Fish, and Konowalow [33] connected at  $R = 35 a_0$  to the long-range asymptotic form

$$D_\infty(R) = D_0 + \frac{b}{R^3}. \quad (8)$$

The value of the coefficient  $D_0$  was  $3.3175$  for both X–A and X–B transitions and the coefficient  $b$  was  $283.07$  or  $-141.53$  [15] for, respectively, X–A or X–B transitions. For both transitions, we multiplied  $D_\infty(R)$  calculated using the above coefficients by a constant such that the value  $D_\infty(35)$  was identical to the corresponding *ab initio* value from Ref. [33] to provide a smooth connection between short and long-range forms for  $D(R)$ . The X–A dipole moment function that we adopted is consistent with that derived by Baumgartner *et al.* [35] from experimental measurements. There is no experimentally-derived dipole moment function for the X–B transition.

#### IV. RESULTS

Bound and continuum wave functions were calculated using the Numerov method to integrate Eq. (3). For the X and A states, eigenvalues were generally in good agreement with the Rydberg-Klein-Rees values used as input to the potentials constructed. [There is an apparent misprint for the energy of the  $v'' = 9$  level of the  $X^1\Sigma_g^+$  state in Ref. [24]. We used  $3\,098.641\,2 \text{ cm}^{-1}$ , consistent with Ref. [29].] The constructed  $B^1\Pi_u$  state potential can reproduce the rotationless IPA energies tabulated by Hessel and Vidal typically to about  $0.1 \text{ cm}^{-1}$ , with the greatest discrepancy  $0.15 \text{ cm}^{-1}$  for the  $v' = 13$  value. Calculated frequencies of  $B^1\Pi_u - X^1\Sigma_g^+$  transitions were also compared with calculations of Verma, Koch, and Stwalley [36] and the agreement was good, within  $0.1 \text{ cm}^{-1}$ . Four quasi-bound levels of

the  $B^1\Pi_u$  state were found. For the rotationless potential their calculated eigenvalues are 143.91, 276.7, 391.74 and 483.88  $\text{cm}^{-1}$  above the dissociation limit for  $v' = 14$  to  $v' = 17$ .

The calculated term energies of vibration-rotation states in the  $X^1\Sigma_g^+$  state were used to compute partition functions using Eq. (5). The maximum vibrational and rotational quantum numbers in our calculations are 41 and 123, respectively, for the  $X^1\Sigma_g^+$  state. In the harmonic approximation for ro-vibrational energies, the partition function can be calculated using the simple expression

$$\begin{aligned} \tilde{Z}_l \equiv Z_R Z_v \approx & \sum_{J''=0}^{123} \omega_{J''} (2J'' + 1) \exp[-hcB_e J''(J'' + 1)/kT] \\ & \times \sum_{v''=0}^{41} \exp[-hv_e(v'' + 1/2)/kT], \end{aligned} \quad (9)$$

which assumes that the term energy can be described by the first terms of the power series with respect to vibrational and rotational quantum numbers. Using constants  $\nu_e/c = 351.3904 \text{ cm}^{-1}$  and  $B_e = 0.672\,566 \text{ cm}^{-1}$  [32] the partition function from Eq. (9) was calculated and it is compared with the partition function calculated from Eq. (5) for the  $X^1\Sigma_g^+$  state as a function of temperature in Fig. 2. The anharmonicity of the potential for higher vibrational levels accounts for the differences between the two results with increasing temperature. For  $J > 2$  the  $X^1\Sigma_g^+$  state supports quasibound vibrational levels. The expression Eq. (5) for  $Z_l$  does not specify whether quasibound states are to be included or not in the summations. We evaluated  $Z_l$  with and without the quasibound levels to ascertain their importance and the results are shown in Fig. 2. The effect of the additional levels becomes increasingly significant with higher temperature. For the present study covering temperatures between 1000 and 2000 K there is not a significant distinction between  $Z_l$ ,  $\tilde{Z}_l$ , and the result with the inclusion of the quasibound states.

The molecular fraction can be calculated using the expression

$$[N_{\text{Li}_2}]/[N_{\text{Li}}]^2 = (Q_{\text{Li}_2}/Q_{\text{Li}}^2) \exp(D_e/kT), \quad (10)$$

where the atomic partition function  $Q_{\text{Li}}$  is  $2(2\pi m_{\text{Li}} kT/h^2)^{3/2}$ , with the electronic partition function for the atom well-approximated by the spin degeneracy of 2 for the temperatures studied in the present work, and the molecular partition function  $Q_{\text{Li}_2}$  is  $(2\pi m_{\text{Li}_2} kT/h^2)^{3/2} Z_l$ , with the electronic partition function for the  $X^1\Sigma_g^+$  state taking the value 1. The molecular fraction Eq. (10) is plotted in Fig. 2. The absorption coefficient  $k(\nu)$  can be obtained if the atomic density is known from

$$k(\nu) = [N_{\text{Li}_2}] \sigma(\nu). \quad (11)$$

## A. Lifetimes

Lifetimes of the various ro-vibrational levels of the  $A^1\Sigma_u^+$  state were measured [35] and calculated, see for example, Refs. [37,38,22]. We calculated spontaneous emission transition probabilities and lifetimes of rotational-vibrational levels of the  $A^1\Sigma_u^+$  state in order to test the adopted transition dipole moment. The spontaneous emission rate from a bound state  $(v'J'\Lambda')$  to a bound state  $(v''J'\Lambda'')$  is

$$A(v'J'\Lambda'; v''J'\Lambda'') = \frac{64\pi^4\nu^3}{3hc^3} g |\langle \phi_{v''J'\Lambda''} | D(R) | \phi_{v'J'\Lambda'} \rangle|^2, \quad (12)$$

where the electronic state degeneracy is

$$g = \frac{(2 - \delta_{0,\Lambda'+\Lambda''})}{2 - \delta_{0,\Lambda'}} \quad (13)$$

and we have neglected change in the rotational quantum number. The total spontaneous emission rate from the upper level  $(v'J'\Lambda')$  can be obtained by summing over all possible transitions to bound and continuum states

$$A(v'J'\Lambda') = \sum_{v''\Lambda''} A(v'J'\Lambda'; v''J'\Lambda'') + \sum_{\Lambda''} \int d\epsilon'' A(v'J'\Lambda'; \epsilon''J'\Lambda''), \quad (14)$$

where  $A(v'J'\Lambda'; \epsilon''J'\Lambda'')$  is the spontaneous emission probability to a continuum energy  $\epsilon''$  with partial wave  $J'$ . The lifetime is

$$\tau = 1/A(v'J'\Lambda'). \quad (15)$$

Lifetimes of levels  $v'J'$  of the  $A^1\Sigma_u^+$  state were measured by Baumgartner *et al.* [35]. The  $A^1\Sigma_u^+$  state is affected by indirect predissociation via the  $a^3\Sigma_u^+$  and  $1^3\Pi_u^+$  states [39,40]. The measured lifetimes  $\tau_m$  of vibration-rotation levels thought to be unaffected by indirect predissociation taken from Ref. [35] and corresponding calculated lifetimes  $\tau_c$  are presented in Fig. 3 along with calculated term energies expressed relative to the potential minimum of the A state. The energies are plotted in the order of the values listed in Table 1 of Ref. [35] and correspond to a range of values of  $(v', J')$  from (0,15) to (24,25). The agreement between  $\tau_c$  and  $\tau_m$  is good within the experimental precision of  $\pm 2$  percent [35]. The quasi-bound levels and continua of the  $X^1\Sigma_g^+$  state inside or above the high centrifugal potential barriers are found to be important in calculating lifetimes of high  $J$  levels. For instance, by including transitions to three quasi-bound levels and the continuum states the calculated lifetime of the  $A^1\Sigma_u^+$  ( $v' = 20, J' = 50$ ) level changes from 22.7 ns to 19.3 ns which is close to the measured lifetime of  $18.66 \pm 0.37$  ns [35]. The calculated and measured lifetimes agree well up to about

4 500  $\text{cm}^{-1}$  in agreement with the findings of Ref. [30]. From approximately 5 000  $\text{cm}^{-1}$  and higher the experimental lifetimes slightly decrease relative to theory by about 0.8 ns or five percent, as demonstrated in Fig. 3. We investigated whether the  $2^1\Sigma_g^+$  state might supply an additional spontaneous decay channel, but the theoretical value  $T_e = 20\,128\text{ cm}^{-1}$  [30] for this state appears to place its minimum at around 6 000  $\text{cm}^{-1}$  relative to the minimum of the  $A^1\Sigma_u^+$  state, apparently ruling this mechanism out. The reason for the significant downturn of experimental lifetimes for higher term energies is currently not understood; however, the overall excellent agreement between our calculated lifetimes and the measurements gives us confidence in our molecular data and calculational procedures. We compare selected examples from the present results with calculations by Watson [37] and by Sangfelt *et al.* [38] in Table I. The calculations of Sangfelt *et al.* are larger than ours, probably because theoretical transition energies were used. A simple rescaling using experimental energies, as pointed out by those authors, yields lifetimes in good agreement with the present work. The dipole moment function calculated by Watson [37] is in good agreement with that adopted in the present study and cannot account for the shorter lifetimes obtained in that study. We present a more extensive tabulation of  $A^1\Sigma_u^+$  lifetimes in Table II covering the same values tabulated in Table VII of Ref. [38].

Lifetimes for levels of the  $B^1\Pi_u$  state have been calculated by Uzer, Watson, and Dalgarno [41], Uzer and Dalgarno [39], and Sangfelt *et al.* [38] and there appear to be no experimental data. In Table III we compare our calculated lifetimes of selected  $B^1\Pi_u$  levels with available calculations for higher values of  $J'$ . The present results lie between the calculations of Uzer *et al.* [41] and those of Sangfelt *et al.* [38]. The lifetimes calculated by Uzer *et al.* are longer than ours because their transition dipole moment function, calculated using a model potential method, is smaller than the *ab initio* dipole moment of Ratcliff *et al.* [33] adopted in the present study. The dipole moment function calculated by Sangfelt *et al.*, on the other hand, is in good agreement with that adopted in the present work. As those authors pointed out, and as our results illustrate, the utilization in their calculation of calculated excitation energies which were larger than experimental energies yielded lifetimes that were too short. In Table IV we present a more extensive tabulation of  $B^1\Pi_u$  lifetimes covering the same values tabulated in Table VIII of Ref. [38].

## B. Absorption cross sections

Absorption spectra arising from molecular singlet transitions at the far wings of the atomic 2p line at 671 nm consist of a blue wing due to  $X^1\Sigma_g^+ - B^1\Pi_u$  transitions and a



red wing due to  $X^1\Sigma_g^+ - A^1\Sigma_u^+$  transitions. Calculations for bound-bound (bb) and bound-free (bf) absorption cross sections were carried out separately using Eq. (4) with  $\Delta\nu = 8 \text{ cm}^{-1}$ . The results for the total (the sum of bb and bf) absorption cross sections at temperatures of 1000 K, 1500 K and 2033 K are given in Figs. 4–6. The ratios of the peak cross sections of the  $X^1\Sigma_g^+ - B^1\Pi_u$  wing to those of the  $X^1\Sigma_g^+ - A^1\Sigma_u^+$  wing are higher at lower temperatures. As temperature increases, absorption spectra spread out from the peak spectral regions and there emerges near 900 nm a satellite feature arising from the minimum [42] in the  $X^1\Sigma_g^+ - A^1\Sigma_u^+$  difference potential and the maximum of the transition dipole moment function [43,33]. We also show the bf contributions to the cross sections on each plot. The bf component contributes mainly to the extreme blue part of the blue wing and increases in magnitude significantly as the temperature increases. It is found that transitions to quasibound and continuum levels of the  $B^1\Pi_u$  state contribute significantly to the total absorption spectra in the case of  $X^1\Sigma_g^+ - B^1\Pi_u$  transitions, apparently because there is less vibrational oscillator strength density in the discrete part of the spectrum for the B state compared to the A state. Transitions into quasibound states of the  $A^1\Sigma_u^+$  or  $B^1\Pi_u$  states have been included in the results for the total cross sections in Figs. 4–6.

Theoretical quantum-mechanical calculations for absorption cross sections from the  $X^1\Sigma_g^+$  state to the  $A^1\Sigma_u^+$  state over the spectral range 600–950 nm were carried out by Lam *et al.* [7] using a constant dipole moment of 6.58 D at 1020 K, for which bf transitions are not significant. Our calculations in Fig. 4 are about a factor of 10 less than the result shown in Fig. 5 of Ref. [7], but agree well both in overall shape and in details of finer structures. We repeated the calculations using the constant dipole moment of Ref. [7] for both classical and quantum-mechanical cross sections and although these two results agreed with each other, they were also a factor of 10 less than the result shown in Fig. 5 of Ref. [7]. Thus it appears to us that there may be a mislabeling of the vertical axis in Fig. 5 of Lam *et al.* [A similar calculation that we performed [44] for  $\text{Na}_2$  at 800 K is in complete agreement with Fig. 4 of Ref. [7].]

Calculations of absorption spectra at 2033 K over the spectral range 450–750 nm presented in Fig. 6 are in good agreement with the measured values of Erdman *et al.* [4] and with quantum-mechanical calculations performed by Mills [11]. The experimental study of Erdman *et al.* [4] involved an investigation of molecular triplet states [4] and did not explore the satellite feature at 900 nm. The calculations over the range 450–750 nm by Mills [11] included triplet molecular transitions and are not directly comparable with the present results. Nevertheless since the singlet transitions dominate the absorption we find excellent qualitative agreement with the calculations presented by Mills.

## ACKNOWLEDGMENTS

We thank R. Côté for generously sharing assembled data and A. Dalgarno for helpful discussions. We also are grateful to A. Gallagher, W. Stwalley, and M. Fajardo for helpful correspondence. This work is supported in part by the National Science Foundation under grant PHY97-24713 and by a grant to the Institute for Theoretical Atomic and Molecular Physics at Harvard College Observatory and the Smithsonian Astrophysical Observatory.

TABLES

TABLE I. Comparison of calculated lifetimes in ns for ro-vibrational levels of the A  $^1\Sigma_u^+$  state.

$v'$	$J'$	Watson [37]	Sangfeldt <i>et al.</i> [38]	This work
7	15	16.8	19.25	18.55
9	5	16.9	19.29	18.65
20	8	17.3		19.04

TABLE II. Lifetimes in ns for ro-vibrational levels of the A  $^1\Sigma_u^+$  state calculated as described in the text.

$v'$	$J' = 0$	$J' = 9$	$J' = 15$
0	17.74	17.77	17.82
1	17.87	17.90	17.94
2	17.98	18.01	18.06
3	18.09	18.12	18.17
4	18.20	18.23	18.27
5	18.30	18.33	18.37
6	18.39	18.42	18.46
7	18.48	18.51	18.55

TABLE III. Comparison of calculated lifetimes in ns for ro-vibrational levels of the  $B^1\Pi_u$  state.

$v'$	$J'$	Uzer <i>et al.</i> [41]	Sangfeldt <i>et al.</i> [38]	This work
0	15	8.3	6.83	7.66
5	9	8.5	7.20	7.95

TABLE IV. Lifetimes in ns for vibrational-rotational levels of the  $B^1\Pi_u$  state calculated as described in the text.

$v'$	$J' = 1$	$J' = 9$	$J' = 15$
0	7.65	7.65	7.66
1	7.70	7.71	7.72
2	7.76	7.76	7.77
3	7.81	7.82	7.83
4	7.88	7.89	7.90
5	7.94	7.95	7.97
6	8.02	8.03	8.04
7	8.10	8.10	8.12

FIGURES

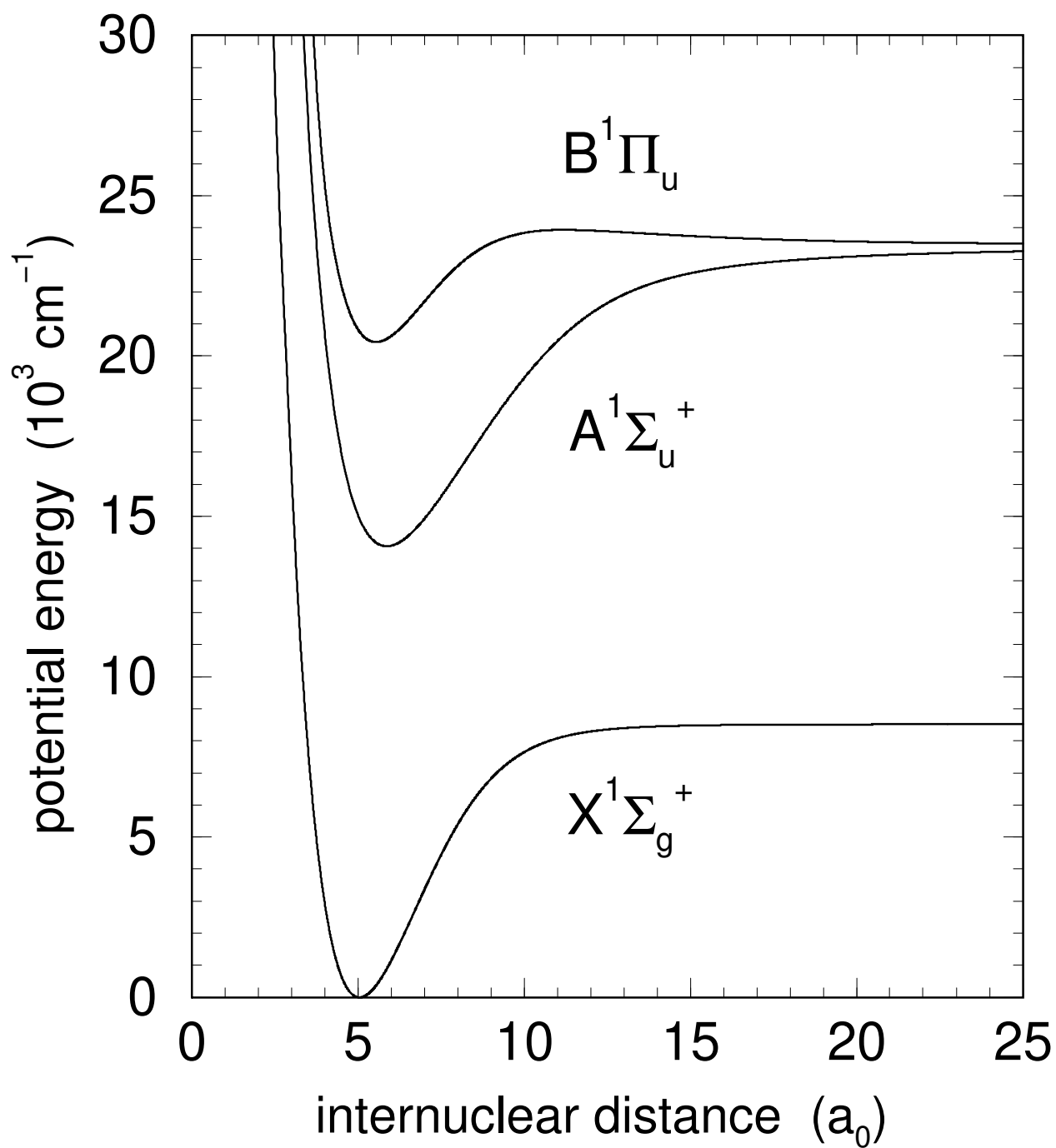


FIG. 1. Adopted potentials for the X<sup>1</sup>Σ<sub>g</sub><sup>+</sup>, A<sup>1</sup>Σ<sub>u</sub><sup>+</sup>, and B<sup>1</sup>Π<sub>u</sub> electronic states.

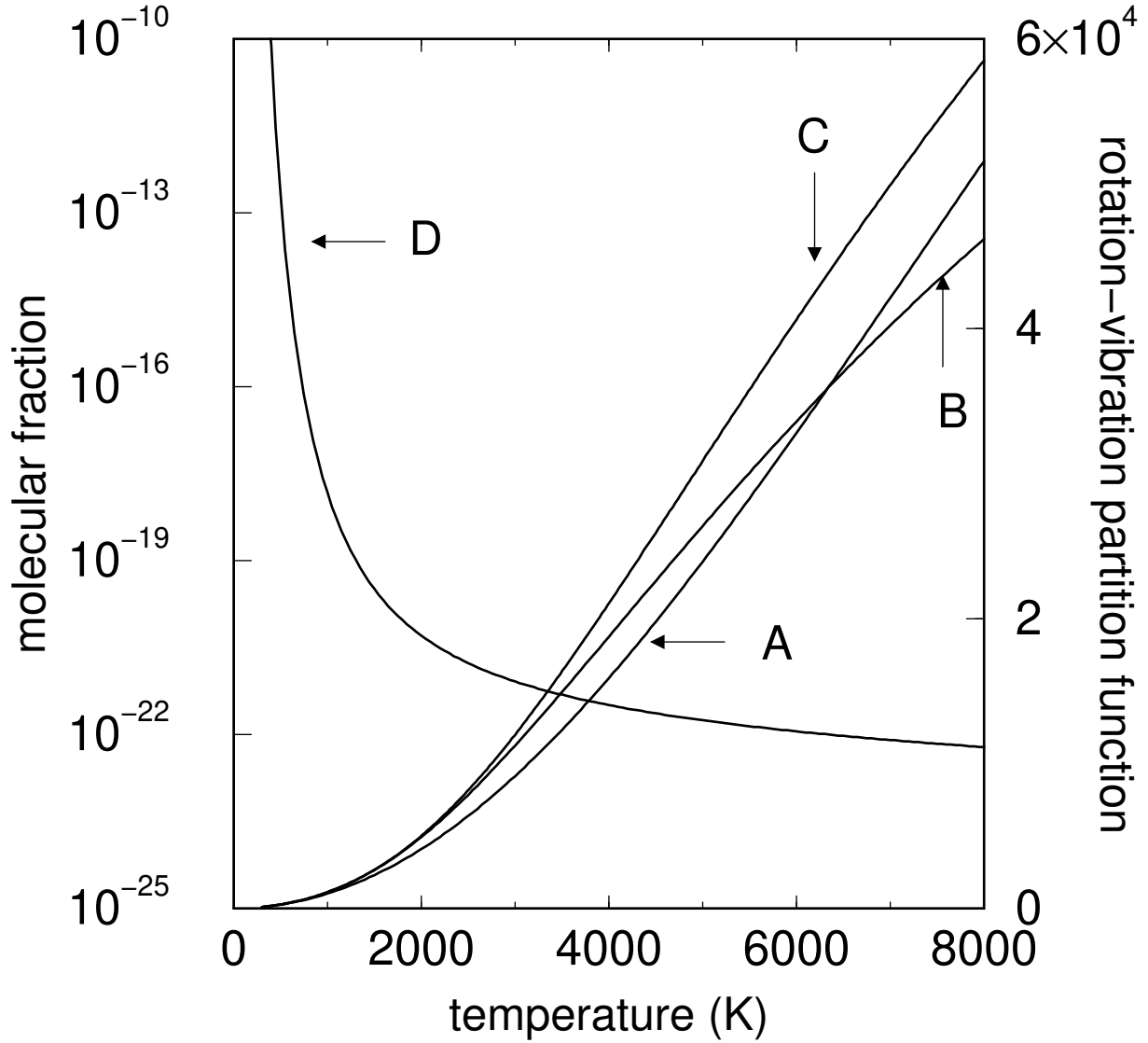


FIG. 2. Comparison at various temperatures of the partition functions  $\tilde{Z}_l$ , calculated using Eq. (9) and experimentally determined spectroscopic constants, curve A, and  $Z_l$ , from Eq. (5) and numerically determined eigenvalues, curves B and C. Inclusion of quasibound states in the calculation of  $Z_l$  results in curve C as discussed in the text. Curve D represents the molecular fraction  $[N_{\text{Li}_2}]/[N_{\text{Li}}]^2$ , Eq. (10), as a function of temperature.

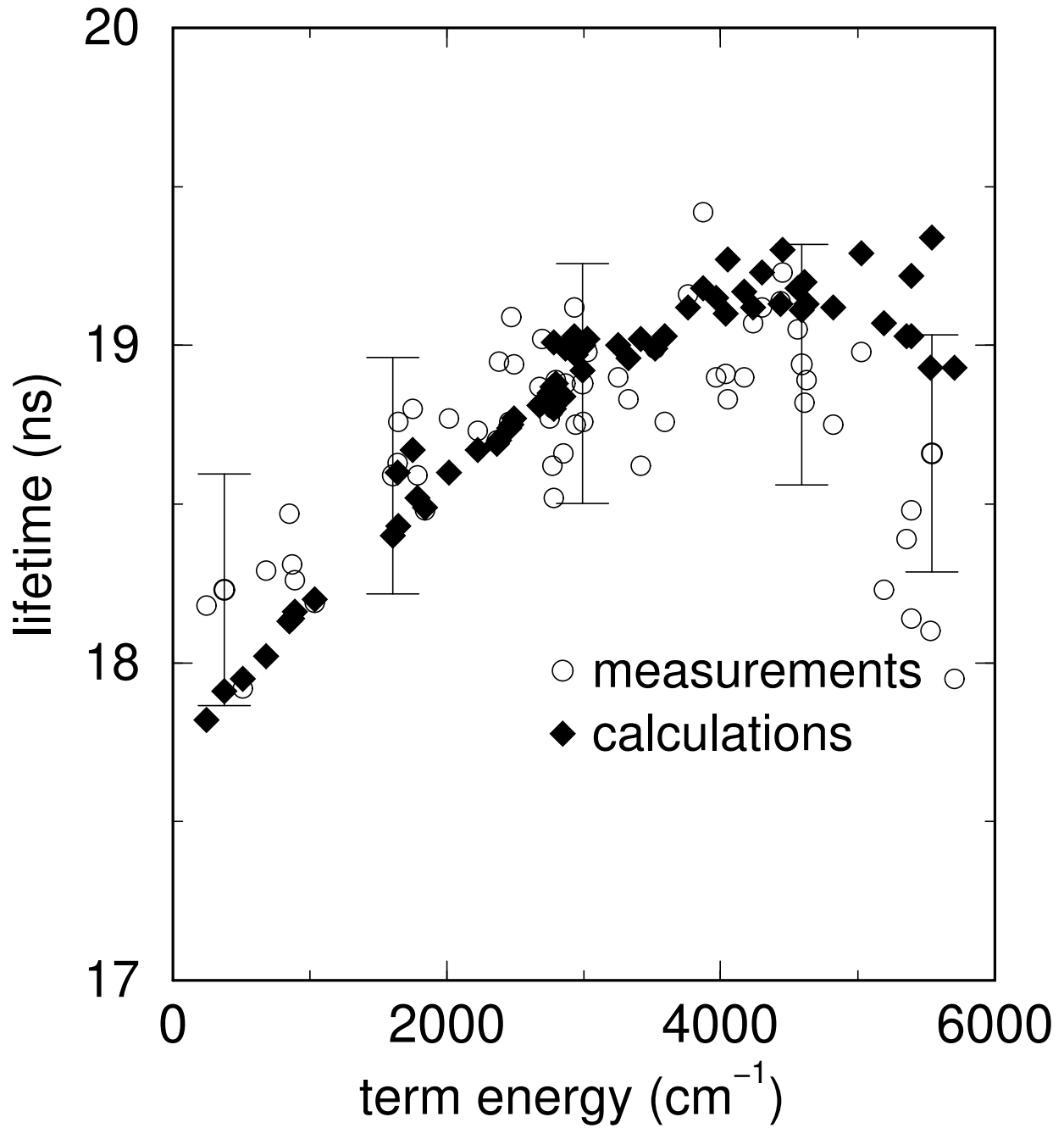


FIG. 3. Comparison of our calculated lifetimes (diamonds) and measured lifetimes (circles) from Ref. [35]. The error bars indicate the quoted experimental uncertainty of  $\pm 2$  percent. The levels given are those that were measured, ordered by increasing energy, as listed in Table 1 of Ref. [35].

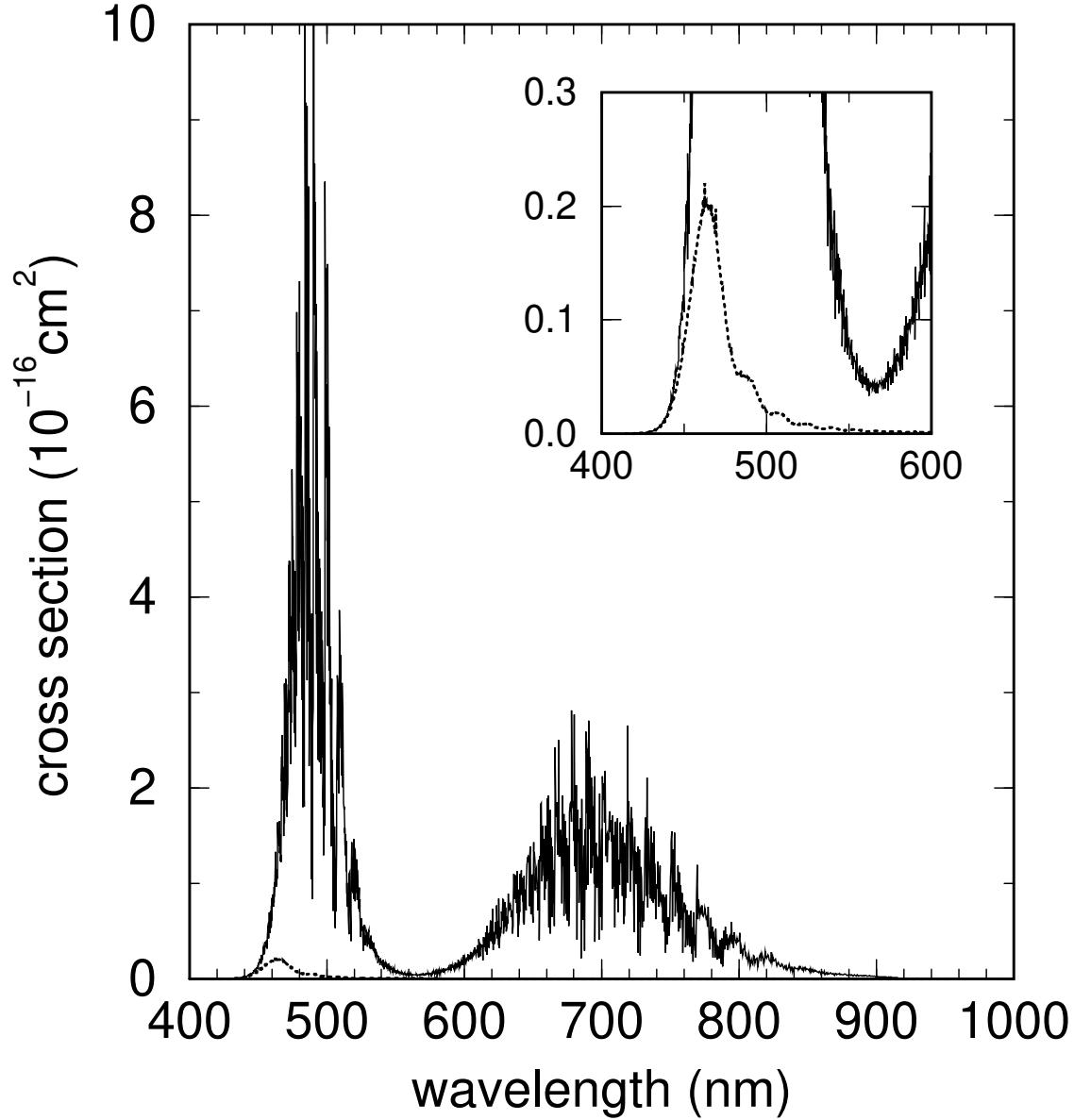


FIG. 4. Total absorption cross sections from  $X^1\Sigma_g^+ - A^1\Sigma_u^+$  and  $X^1\Sigma_g^+ - B^1\Pi_u$  transitions including bound to bound and bound to free transitions at a temperature of 1000 K. The satellite feature near 900 nm does not appear at this temperature and bound-free absorption (dotted curve) is insignificant. The inset presents a magnified view of the bound-free contribution.



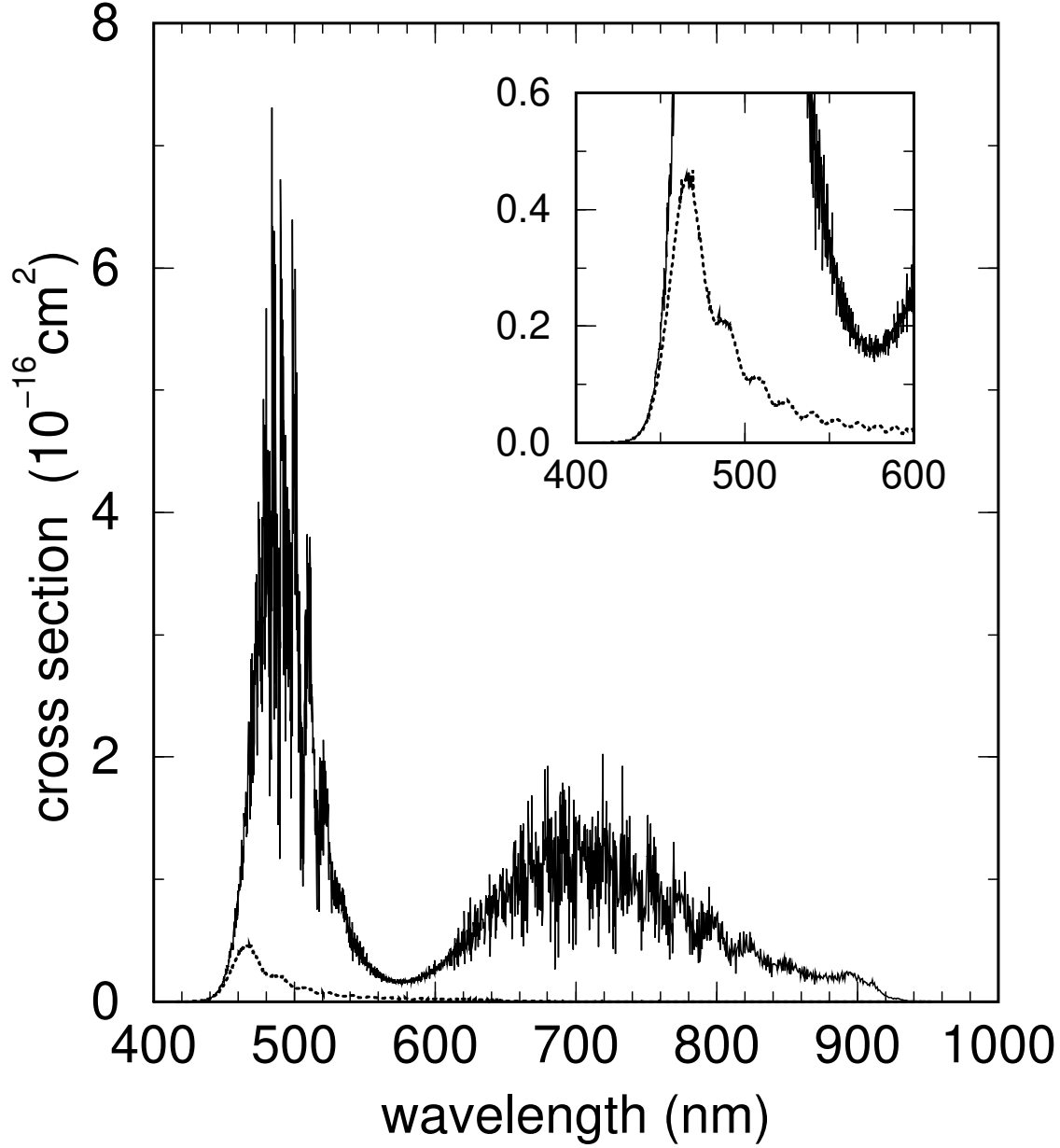


FIG. 5. Total absorption cross sections from  $X^1\Sigma_g^+-A^1\Sigma_u^+$  and  $X^1\Sigma_g^+-B^1\Pi_u$  transitions including bound to bound and bound to free transitions at a temperature of 1500 K. As the temperature increases, the absorption spectra are distributed over a wider spectral range and the ratio of the peak cross sections between  $X^1\Sigma_g^+-B^1\Pi_u$  and  $X^1\Sigma_g^+-A^1\Sigma_u^+$  bands decreases. The satellite feature near 900 nm and bound-free absorption (dotted curve) are noticeable at this temperature. The inset presents a magnified view of the bound-free contribution.

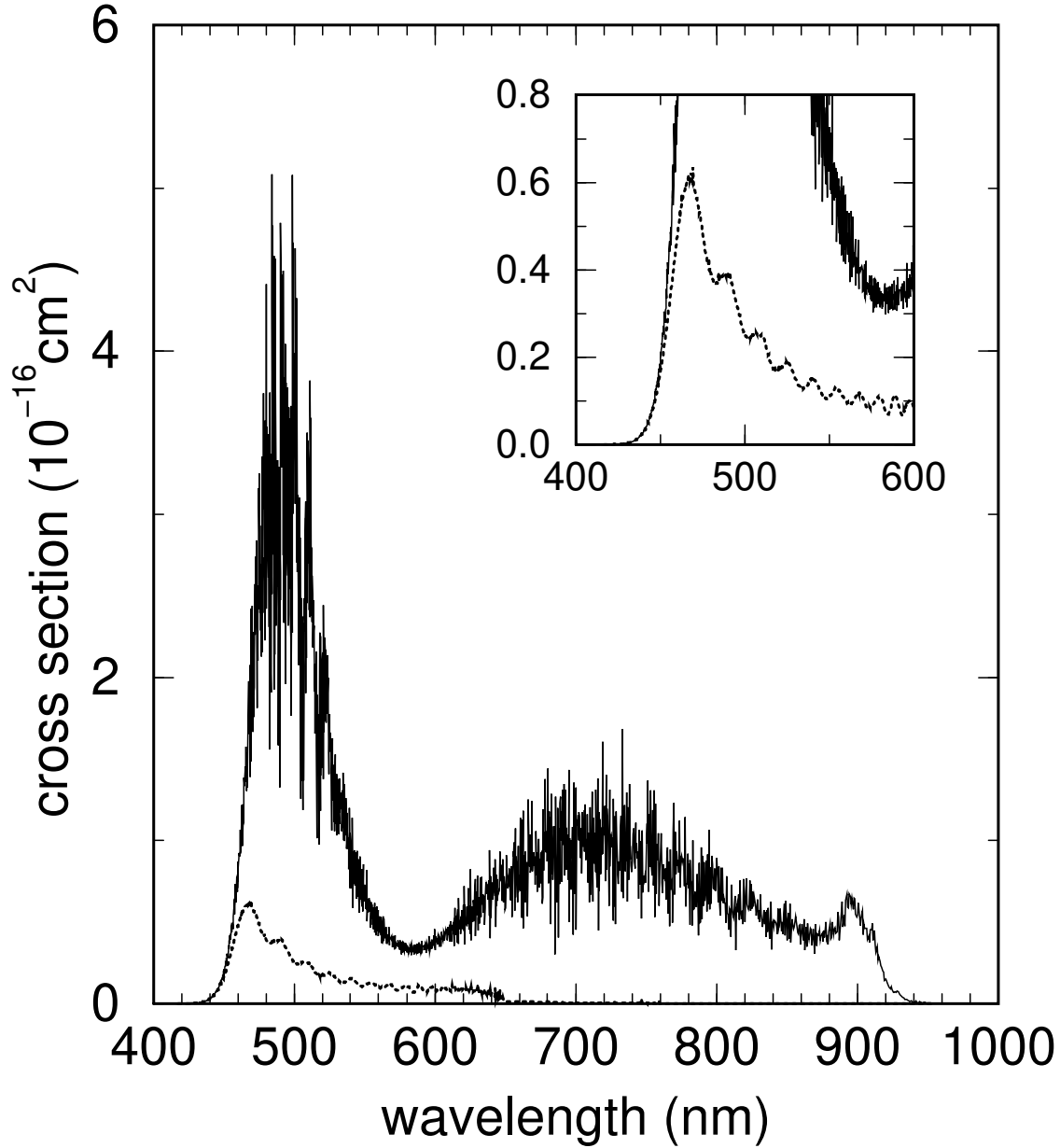


FIG. 6. Total absorption cross sections from  $X^1\Sigma_g^+ - A^1\Sigma_u^+$  and  $X^1\Sigma_g^+ - B^1\Pi_u$  transitions including bound to bound and bound to free transitions at a temperature of 2033 K. At this temperature the satellite feature near 900 nm is now prominent and bound-free absorption (dotted curve) contributes significantly at 450 nm. The inset presents a magnified view of the bound-free contribution.

## REFERENCES

- [1] C. R. Vidal, *J. Appl. Phys.* **44**, 2225 (1973).
- [2] D. Vezã, S. Milošević, and G. Pichler, *Chem. Phys. Lett.* **93**, 401 (1982).
- [3] W. Theiss, H. J. Müschenborn, and W. Demtröder, *Chem. Phys. Lett.* **174**, 126 (1990).
- [4] P. S. Erdman *et al.*, *Chem. Phys. Lett.* **252**, 248 (1996).
- [5] D. R. Bates, *Mon. Not. R. Astron. Soc.* **112**, 40 (1952).
- [6] J. Szudy and W. E. Baylis, *J. Quant. Spectr. Rad. Trans.* **15**, 641 (1975).
- [7] L. K. Lam, A. Gallagher, and M. M. Hessel, *J. Chem. Phys.* **66**, 3550 (1977).
- [8] J. Schlejen, J. P. Woerdman, and G. Pichler, *J. Mol. Spect.* **128**, 1 (1988).
- [9] J. P. Woerdman *et al.*, *J. Phys. B* **18**, 4205 (1985).
- [10] R. A. Buckingham, S. Reid, and R. Spence, *Mon. Not. R. Astron. Soc.* **112**, 382 (1952).
- [11] J. D. Mills, Technical Report No. PL-TR-94-3001, Propulsion Directorate, Phillips Laboratory, Air Force Materiel Command (unpublished).
- [12] R. Côté and A. Dalgarno, *Phys. Rev. A* **50**, 4827 (1994).
- [13] E. R. I. Abraham, W. I. McAlexander, C. A. Sackett, and R. G. Hulet, *Phys. Rev. Lett.* **74**, 1315 (1995).
- [14] E. R. I. Abraham *et al.*, *Phys. Rev. A.* **53**, R3713 (1996).
- [15] M. Marinescu and A. Dalgarno, *Phys. Rev. A* **52**, 311 (1995).
- [16] Z.-C. Yan, A. Dalgarno, and J. F. Babb, *Phys. Rev. A* **55**, 2882 (1997).
- [17] F. Martin *et al.*, *Phys. Rev. A* **55**, 3458 (1997).
- [18] Z.-C. Yan and G. W. F. Drake, *Phys. Rev. A* **52**, R4316 (1995).
- [19] E. R. I. Abraham *et al.*, *Phys. Rev. A.* **54**, R5 (1996).
- [20] H. Friedrich, *Theoretical Atomic Physics* (Springer, Berlin, 1991).
- [21] H. Lefebvre-Brion and R. W. Field, *Perturbations in the spectra of diatomic molecules* (Academic, Orlando, 1986).
- [22] R. Côté and A. Dalgarno, *Phys. Rev. A* **58**, 498 (1998).

- [23] W. T. Zemke and W. C. Stwalley, *J. Phys. Chem.* **97**, 2053 (1993).
- [24] B. Barakat *et al.*, *Chem. Phys.* **102**, 215 (1986).
- [25] B. Bussery and M. Aubert-Frécon, *J. Chem. Phys.* **82**, 3224 (1985).
- [26] Z.-C. Yan, J. F. Babb, A. Dalgarno, and G. W. F. Drake, *Phys. Rev. A* **54**, 2824 (1996).
- [27] M. Rérat, B. Bussery, and M. Frécon, *J. Mol. Spect.* **182**, 260 (1997).
- [28] J. Weiner, V. S. Bagnato, S. Zilio, and P. S. Julienne, *Rev. Mod. Phys.* **71**, 1 (1999).
- [29] P. Kusch and M. M. Hessel, *J. Chem. Phys.* **67**, 586 (1977).
- [30] I. Schmidt-Mink, W. Müller, and W. Meyer, *Chem. Phys.* **92**, 263 (1985).
- [31] M. L. Olson and D. D. Konowalow, *Chem. Phys.* **22**, 29 (1977).
- [32] M. M. Hessel and C. R. Vidal, *J. Chem. Phys.* **70**, 4439 (1979).
- [33] L. B. Ratcliff, J. L. Fish, and D. D. Konowalow, *J. Molec. Spectrosc.* **122**, 293 (1987).
- [34] D. D. Konowalow, M. E. Rosenkrantz, and D. S. Hochhauser, *J. Mol. Spect.* **99**, 321 (1983).
- [35] G. Baumgartner, H. Kornmeier, and W. Preuss, *Chem. Phys. Lett.* **107**, 13 (1984).
- [36] K. K. Verma, M. E. Koch, and W. C. Stwalley, *J. Chem. Phys.* **78**, 3614 (1983).
- [37] D. K. Watson, *Chem. Phys. Lett.* **51**, 513 (1977).
- [38] E. Sangfelt, H. A. Kurtz, N. Elander, and O. Goscinski, *J. Chem. Phys.* **81**, 3976 (1984).
- [39] T. Uzer and A. Dalgarno, *Chem. Phys.* **51**, 271 (1980).
- [40] I. Schmidt-Mink and W. Meyer, *Chem. Phys. Lett.* **121**, 49 (1985).
- [41] T. Uzer, D. K. Watson, and A. Dalgarno, *Chem. Phys. Lett.* **55**, 6 (1978).
- [42] A. Jabłonski, *Phys. Rev.* **68**, 78 (1945).
- [43] J. P. Woerdman, *J. Chem. Phys.* **75**, 5577 (1981).
- [44] H.-K. Chung, K. Kirby, and J. F. Babb, in preparation (unpublished).